JAERI-M
89-165

NUMERICAL SIMULATION OF OPERATION REGION IN JT-60 OHMIC PLASMA

October 1989

Katsuhiro SHIMIZU, Hiroshi SHIRAI, Toshio HIRAYAMA and Masafumi AZUMI

日本原子力研究所
Japan Atomic Energy Research Institute

JAERI-Mレポートは，日本原子力研究所が不定期に公刊している研究報告書です。
入手の問合わせは，日本原子力研究所技術情報部情報資料課（〒319-11茨城県那珂郡東海村）あて，お申しこしください。なお，このほかに財団法人原子力弘済会資料センター（〒319-11茨城県那珂郡東海村日本原子力研究所内）で複写による実費頒布をおこなっております。

JAERI-M reports are issued irregularly.
Inquiries about availability of the reports should be addressed to Information Division Department of Technical Information, Japan Atomic Energy Research Institute, Tokai-mura, Naka-gun, Ibaraki-ken 319-11, Japan.

編集兼発行　日本原子力研究所
印　　刷　いばらき印刷㈱

JAERI-M 89-165

Numerical Simulation of Operation Region in JT-60 Ohmic Plasma

Katsuhiro SHIMIZU, Hiroshi SHIRAI, Toshio HIRAYAMA
and Masafumi AZUMI

Department of Large Tokamak Research
Naka Fusion Research Establishment
Japan Atomic Energy Research Institute
Naka-machi, Naka-gun, Ibaraki-ken

(Received September 29, 1989)

The stable operation region for a major disruption has been numerically investigated, for joule heated plasmas of JT-60, by using a tokamak transport code including both effects of the MHD instability and the non-coronal radiation cooling. The overlapping of the m/n = 2/1 and 3/2 magnetic islands or the contact of the m/n = 2/1 island with a limiter are used as the condition for the occurrence of a major disruption. The density limit obtained from the simulation qualitatively agrees with experimental results. It is found that the sawtooth oscillation plays an important role in driving the tearing modes unstable.

Keywords: Numerical Simulation, JT-60, Operation Region, Major Disruption, Sawtooth Oscillation, Tearing Mode

JAERI－M 89－165

JT－60オーミック・プラズマのオペレイション領域についての数値シミュレーション

日本原子力研究所那珂研究所臨界プラズマ研究部
清水　勝宏・白井　　浩・平山　俊雄・安積　正史

（1989年9月29日受理）

JT－60のOH加熱時の安定な放電領域について，トカマク輸送コードを用いた数値シミュレーションによって調べた。このコードには，MHD不安定性と輸送との相互作用，不純物による放射損失の効果が組み込まれている。m／n＝2／1のティアリング・モードによる磁気島がリミターに接触したり，2／1と3／2モードの磁気島が重なった時を，破壊型不安定性が生じる条件として用いる。シミュレーションによって得られた密度限界は，実験データと定性的に一致している。プラズマ中心部での電流値を制限する鋸歯状振動が，ティアリング・モードを励起するのに重要な役割をはたしている事がわかった。

那珂研究所：〒311－01　茨城県那珂郡那珂町大字向山801－1

Contents

1. Introduction 1
2. Model 2
2.1 Transport equation 2
2.2 Impurity transport 3
2.3 Tearing mode 4
2.4 Sawtooth oscillation 5
3. Simulation Result 6
3.1 Low-q operation in the steady state 6
3.2 Current ramp-up phase 7
3.2 Density limit 9
4. Summary and Discussion 11
Acknowledgments 12
References 13

目　　次

1. 序　論 1
2. 計算モデル 2
2.1 輸送方程式 2
2.2 不純物輸送 3
2.3 ティアリング・モード 4
2.4 鋸歯状振動 5
3. シミュレーション結果 6
3.1 低安全係数放電の定常状態 6
3.2 電流立ち上げ時 7
3.3 密度限界 9
4. 総括と議論 11
謝　辞 12
参考文献 13

1. Introduction

To obtain a high beta plasma with high plasma current is one of the most important objectives in the thermonuclear fusion research by tokamak. However, when the high current and/or high density operation are carried out to achieve a high beta plasma, the discharge frequently terminates by a disruption. Major disruption limits the plasma density and the plasma current in tokamak experiments [1, 2]. In the reactor grade tokamak, the disruption may cause a serious damage to the first wall. Therefore, it is very important to comprehend the mechanism of the major disruption and to suppress it. The destruction of magnetic surface extended over a plasma column has been considered to cause the disruption. The theoretical analysis and numerical simulation with MHD code suggest two plausible conditions of occurrence of disruption; one is the contact of m/n = 2/1 island produced by tearing mode with a limiter [3], where m and n are the poloidal and toroidal mode numbers, respectively; and the other is the overlapping of 2/1 island with 3/2 island [4,5]. To examine these criteria for the major disruption is significant as an effort to find the way to control the disruption.

As the first step, we investigate numerically the stable operation region for joule heated plasma of JT-60 by using a tokamak transport code [6,7]. The transport code includes the model to simulate the sawtooth oscillation, the MHD effects on the transport and the cooling effect by non-coronal impurity radiation. We investigate the possibility of the low-q operation ($q_a < 3$, where q_a is the safety factor at plasma surface). The simulation result shows that the rapid current rise ($dI_p / dt > 0.75$ MA/s) leads to the overlapping of m/n = 2/1 island with 3/2 island. Since the skin current during the current ramp-up phase destabilizes the tearing modes, the carefully controlled gas puffing can suppress the skin current, and consequently, prevent a major disruption . We also study the dependence of the maximum plasma density on the plasma current. The shrink of the current channel due to the surface radiation cooling destabilizes the tearing modes, and causes the overlapping

of 2/1 and 3/2 mode islands. The dependence of this critical density on the plasma current qualitatively agrees with experimental results [8].

2. MODEL

2.1 Transport equation

We solve the following transport equations which consist of particle conservation, electron energy balance, ion energy balance and Maxwell equation for poloidal magnetic fields;

$$\frac{\partial n_e}{\partial t} = -\frac{1}{r}\frac{\partial}{\partial r}(r\Gamma) + S_i \qquad (1)$$

$$\frac{3}{2}\frac{\partial}{\partial t}(n_e T_e) = -\frac{1}{r}\frac{\partial}{\partial r}(r Q_e) + E_z J_z - \frac{3m_e}{m_i}\frac{n_e}{\tau_e}(T_e - T_i) - P_{ion} - P_{rad} \qquad (2)$$

$$\frac{3}{2}\frac{\partial}{\partial t}(n_i T_i) = -\frac{1}{r}\frac{\partial}{\partial r}(r Q_i) + \frac{3m_e}{m_i}\frac{n_e}{\tau_e}(T_e - T_i) - P_{cx} \qquad (3)$$

$$\frac{\partial B_\theta}{\partial t} = \frac{\partial E_z}{\partial r} \qquad (4)$$

$$E_z = \eta_z J_z = \mu_0^{-1}\eta_z \frac{1}{r}\frac{\partial}{\partial r}(r B_\theta) \qquad (5)$$

where n_e, T_e, T_i , B_p are the electron density, electron temperature, ion temperature and the poloidal magnetic field, respectively. The term of S_i , P_{ion} , P_{rad} and P_{cx} denote the particle source, the ionization power loss by neural hydrogen, the electron energy loss by

of 2/1 and 3/2 mode islands. The dependence of this critical density on the plasma current qualitatively agrees with experimental results [8].

2. MODEL

2.1 Transport equation

We solve the following transport equations which consist of particle conservation, electron energy balance, ion energy balance and Maxwell equation for poloidal magnetic fields;

$$\frac{\partial n_e}{\partial t} = -\frac{1}{r}\frac{\partial}{\partial r}(r\Gamma) + S_i \qquad (1)$$

$$\frac{3}{2}\frac{\partial}{\partial t}(n_e T_e) = -\frac{1}{r}\frac{\partial}{\partial r}(r Q_e) + E_z J_z - \frac{3m_e}{m_i}\frac{n_e}{\tau_e}(T_e - T_i) - P_{ion} - P_{rad} \qquad (2)$$

$$\frac{3}{2}\frac{\partial}{\partial t}(n_i T_i) = -\frac{1}{r}\frac{\partial}{\partial r}(r Q_i) + \frac{3m_e}{m_i}\frac{n_e}{\tau_e}(T_e - T_i) - P_{cx} \qquad (3)$$

$$\frac{\partial B_\theta}{\partial t} = \frac{\partial E_z}{\partial r} \qquad (4)$$

$$E_z = \eta_z J_z = \mu_0^{-1}\eta_z \frac{1}{r}\frac{\partial}{\partial r}(r B_\theta) \qquad (5)$$

where n_e, T_e, T_i , B_p are the electron density, electron temperature, ion temperature and the poloidal magnetic field, respectively. The term of S_i , P_{ion} , P_{rad} and P_{cx} denote the particle source, the ionization power loss by neural hydrogen, the electron energy loss by

impurity radiation and the charge exchange loss, respectively. The term E_z is toroidal electric field, J_z is current density, and μ_0 is the vacuum magnetic permeability. For the electric resistivity η_z, we take the neoclassical expression included the effect of trapped electrons. The particle flux Γ and the electron and ion heat fluxes Q_e, Q_i are expressed as follows,

$$\Gamma = - D_e \frac{\partial n_e}{\partial r} - V_{in} n_e \qquad (6)$$

$$Q_e = - n_e \chi_e \frac{\partial T_e}{\partial r} - \frac{3}{2} D_e T_e \frac{\partial n_e}{\partial r} \qquad (7)$$

$$Q_i = - n_i \chi_i \frac{\partial T_i}{\partial r} - \frac{3}{2} D_i T_i \frac{\partial n_i}{\partial r} \qquad (8)$$

Here, V_{in} represents the anomalous inward velocity. We employ the neoclassical expression derived by Chang-Hinton for the ion thermal conductivity χ_i [9]. The INTOR type scaling for the anomalous particle diffusion D_e and the Neo-Alcator scaling [10] for electron energy diffusion χ_e are used,

$$D_e = D_i = 1.0 \times 10^{19} / n_e \qquad (9)$$

$$\chi_e = 4.4 \times 10^{20} \; r / R^2 n_e \qquad (10)$$

The electron thermal conductivity inside the island is enhanced by a large factor of 100. This MHD effects on the transport will be described in section 2.3.

2.2 Impurity transport

The radiation cooling effect is very important for high density operation. So, we solve the following impurity transport equations by combining with the plasma transport [11].

$$\frac{\partial n_k}{\partial t} = -\frac{1}{r}\frac{\partial}{\partial r}(r\Gamma_k) + n_e\alpha_{k-1}n_{k-1} - \left(n_e\alpha_k + n_e\beta_k + n_0\beta_k^{CT}\right)n_k + \left(n_e\beta_{k+1} + n_0\beta_{k+1}^{CT}\right) \qquad (11)$$

where n_k is the number density of impurity ions with (k-1) electric charge, α_k is the rate coefficient for ionization from the state k to k+1 and β_k is the recombination rate coefficient from the state k+1 to k. We use the Hulse's multi-ion model [12] for the ionization and recombination rates. The term of β_k^{CT} represents the charge-transfer recombination [13] with the thermal neutral of density n_0. The anomalous particle flux Γ_k is written in the form of

$$\Gamma_k = -D_A\frac{\partial n_k}{\partial r} - V_A n_k \qquad (12)$$

where D_A is the anomalous diffusion coefficient and V_A is the anomalous pinch velocity. These parameters are taken to be $D_A = 1\ m^2/s$ and $V_A/D_A = C_v\, 2r/a^2$, where a is the minor radius and C_v is called the shape parameter [14]. The value of C_v is taken to be normally 1.0.

2.3 Tearing mode

The stability of tearing mode is examined by solving the following equation for the perturbed helical flux function Ψ [15],

$$\frac{1}{r}\frac{d}{dr}\left(r\frac{d\psi}{dr}\right) = \left(\frac{m^2}{r^2} + \frac{\mu_0\, dJ_z/dr}{B_\theta\,(1 - nq/m)}\right)\psi \qquad (13)$$

$$\Delta'(\varepsilon) = \left(\frac{d\psi}{dr}(r_s+\varepsilon) - \frac{d\psi}{dr}(r_s-\varepsilon) \right) / \psi(r_s) \qquad (14)$$

where r_s is the radius of the resonant surface with the poloidal mode number of m and toroidal mode number of n. When the mode is unstable $\left(\Delta'(0) > 0 \right)$, the island grows with the rate given by Rutherford theory [16,17] as follows,

$$\frac{dW}{dt} = 1.66 \frac{\eta(r_s)}{\mu_0} \Delta'(W) \qquad (15)$$

$$\Delta'(W) = \left(\frac{d\psi}{dr}(r_s+w/2) - \frac{d\psi}{dr}(r_s-w/2) \right) / \psi(r_s) \qquad (16)$$

where W is the width of the island. The island growth saturates when $\Delta'(W) = 0$. The electron thermal conductivity is enhanced by a large factor of 100 inside the island.

$$\chi_e^{ISL}(r) = 100 \times \chi_e \qquad (17)$$

The electron temperature is flattened across the island by this enhanced thermal conductivity; χ_e^{ISL}; as a result, the current density is also flattened.

2.4 Sawtooth oscillation

In order to simulate the sawtooth oscillations, the model similar to that given by Waddel et al. [18] is incorporated into the tokamak code. When the safety factor at the plasma center q_0 is lower than unity, the magnetic island grows around the q = 1 resonant surface as follows,

$$W = W_0 \exp\left(\int \gamma(t)\, dt \right) \qquad (18)$$

where W_0 is initial island width and γ is the linear growth rate including the diamagnetic effect. When the width of this island, W, reaches to the plasma center, the minor disruption occurs and the current density is mixed inside the critical radius r_0 on the basis

of Kadomtsev model [19] as well as the flattening of the electron temperature. After the mixing, the safety factor at the plasma center q_0 becomes unity. As the electron temperature increases at the plasma center by the joule heating, the current begins to concentrate at the plasma center. The safety factor q_0 becomes lower than unity, the magnetic island grows again and then the minor disruption occurs. These process are repeated.

In this model, the period of sawtooth oscillations and the amplitude .e.g. the change of central electron temperature before and after the minor disruption, are determined self-consistently. The simulation result agrees well with the sawtooth oscillation observed in JT-60 Ohmic plasma [20].

3. Simulation Result

The calculation have been carried out to study the requirements for stable low-q operation and the density limit. For the second purpose, we take the radiation cooling effect by impurity into consideration. When the m/n = 2/1 island contacts with a limiter or the 2/1 island and the 3/2 island overlap, a confinement of a plasma is assumed to be lost. The parameter used in the simulations are listed in table 1.

3.1 low-q operation in the steady state

Firstly, we investigate the possibility of low-q operation and the control parameter to stabilize the tearing mode. We solve the transport equations of (1) ~ (5) for I_p = 1 - 2.7 MA. and obtain the current density profile in the steady state. In these calculations, the electron thermal conductivity inside the island, χ_e^{ISL} is not included and the volume-averaged density is fixed at a value of $< n_e > = 3.5 \times 10^{19}$ m^{-3}. For the current density profile obtained, the saturated island width is calculated by solving the equations of (13)

of Kadomtsev model [19] as well as the flattening of the electron temperature. After the mixing, the safety factor at the plasma center q_0 becomes unity. As the electron temperature increases at the plasma center by the joule heating, the current begins to concentrate at the plasma center. The safety factor q_0 becomes lower than unity, the magnetic island grows again and then the minor disruption occurs. These process are repeated.

In this model, the period of sawtooth oscillations and the amplitude .e.g. the change of central electron temperature before and after the minor disruption, are determined self-consistently. The simulation result agrees well with the sawtooth oscillation observed in JT-60 Ohmic plasma [20].

3. Simulation Result

The calculation have been carried out to study the requirements for stable low-q operation and the density limit. For the second purpose, we take the radiation cooling effect by impurity into consideration. When the m/n = 2/1 island contacts with a limiter or the 2/1 island and the 3/2 island overlap, a confinement of a plasma is assumed to be lost. The parameter used in the simulations are listed in table 1.

3.1 low-q operation in the steady state

Firstly, we investigate the possibility of low-q operation and the control parameter to stabilize the tearing mode. We solve the transport equations of (1) ~ (5) for I_p = 1 - 2.7 MA. and obtain the current density profile in the steady state. In these calculations, the electron thermal conductivity inside the island, χ_e^{ISL} is not included and the volume-averaged density is fixed at a value of $< n_e > = 3.5 \times 10^{19}$ m^{-3}. For the current density profile obtained, the saturated island width is calculated by solving the equations of (13)

and (16). Figure 1 shows the dependence of saturated island width on the safety factor at the plasma surface q_a in the steady state. The position of resonant surface of the 1/1 mode is also plotted in this figure. the electron temperature and the current density in the region of $r \leq r_0 \approx 1.2\, r_s$, where r_s is the q = 1 singular surface, are flattened by the sawtooth model described in section 2.3. The m/n = 2/1 island width is sensitive to the wall position r = b, for the low-q operation ($q_a < 3$) . For the case of $q_a = 2.5$, the 2/1 island contacts with the limiter for b/a > 1.5, while the mode is stable for b/a = 1.0. In the standard case, we set the wall at b/a = 1.2. It should be noted that the 2/1 tearing mode is unstable, but the 3/2 mode is always stable without the enhancement of χ_e^{ISL}. The 2/1 island width is nearly constant in the rage of $3.5 < q_a < 7$ but the width increases rapidly with decreasing in $q_a < 3.0$. This result means that the low-q operation is difficult without the stabilizing effect of the conducting wall.

3.2 Current ramp-up phase

The stability of tearing mode in the low-q operation strongly depends on the current rise rate dI_p / dt . Figure 2 shows the time evolution of magnetic islands width during the current rise-phase. Although the 2/1 mode is stabilized in the steady state by the effect of conducting wall placed at close to plasma surface (b/a = 1.0), the rapid current rise ($dI_p / dt > 1.0$ MA/s) increases the current density gradient at the plasma resonant surface and destabilizes this mode. This effect leads to the contact of 2/1 island with a limiter. The critical current rise rate where the m/n = 2/1 island contacts with a limiter depends on the position of the conducting wall. (In the case of b/a = 1.2, the critical current rise rate is $dI_p / dt = 0.75$ MA/s .) The 3/2 mode becomes unstable for the current density profile with a steep gradient, which is produced by the rapid current rise. The skin current which destabilize the tearing mode can be prevented by the surface cooling. The gas-puffing is one of the effective means to cool the plasma edge. However the large gas-puffing ($d\langle n_e \rangle / dt > 2 \times 10^{19}$ m^{-3}/s for $dI_p / dt > 0.75$ MA/s) shrinks the current channel and

leads to the disruption. This phenomena will be shown in section 3.2 related to the density limit.

We investigate the effect of enhanced thermal conductivity inside the magnetic island, χ_e^{ISL}. Figures 3 (a) and (b) shows the simulation results for $dI_p / dt = 0.5$ MA/s without and with χ_e^{ISL}, respectively. The wall position is taken to be b/a = 1.2 hereafter. The enhanced thermal conductivity flatten the electron temperature across the island and reduces the current density gradient at the resonant surface. The island width becomes smaller, and consequently, the disruption can be avoided. But the further increase in current rise leads to a new situation. The time evolution of magnetic islands for $dI_p / dt = 0.75$ MA/s is shown in Fig. 4 (a). The overlapping of 2/1 island and 3/2 island occurs at t = 3.5 sec. The large island of 2/1 mode makes the current density gradient at q = 3/2 resonant surface steep, as shown in Fig. 4 (b). (The dotted line is the current density profile without the enhanced thermal conductivity.) When the sharp gradient appears in J_z (r) profile, the 3/2 mode grows up explosively and the island extends to the 2/1 island, i.e. a major disruption occurs. M.F. Turner and J.A. Wesson [20] have shown that the nonlinear interaction of m = 1 mode and 2/1 mode through the current profile leads to a disruption using the one-dimensional transport code included the MHD effect. However, in our model, the 3/2 mode is always destabilized before the interaction of m = 1 mode and the 2/1 mode and the overlapping occurs.

The effect of edge electron temperature is investigated. The edge plasma parameter ($n_e(a)$, $T_e(a)$, $T_i(a)$) is hitherto fixed at a given value. In this simulation, we solve the transport equation including the scrape off region. The particle and the convective energy loss along the field line are given by $- n / \tau_{\parallel}$, $- \gamma_e n_e T_e / \tau_{\parallel}$ and $- \gamma_i n_i T_i / \tau_{\parallel}$, respectively. Here, $\tau_{\parallel} = \pi q R / v_f$, where $v_f = C_f v_s$ and v_s is the sound velocity and C_f is the numerical factor. The factor of γ_e and γ_i are the energy transmission coefficients across the sheath for electron and ion, respectively. The cross field diffusion in the scrape-off region is assumed to be the Bohm type diffusion. We use the following transport coefficients, $D_e = 0.5\, D_B$, $\chi_e = \chi_i = 0.5\, D_B$, $C_f = 0.5$, $\gamma_e = 5.8$, $\gamma_i = 2.0$.

The edge electron temperature is self-consistently determined by the balance of the parallel loss and the diffusion in the scrape-of region. The figure 5 shows that high boundary temperature increases the current density near the plasma edge and reduces the current density gradient. The 2/1 island width is still large during the current rise but the disruption can be avoided. However this pedestal profile in the current density may drive the kink instability [22]. It is necessary to examine the stability of the kink mode for such a current density profile.

3.2 Density limit

We investigate the dependence of the maximum plasma density on the plasma current. In these simulations, impurity content and plasma current are fixed temporally. Figure 6 shows the time evolution of the volume-averaged density $\overline{n}_e$, the particle-averaged temperature $\overline{T}_e$, $\overline{T}_i$, the joule input power P_{joul} , radiation loss P_{rad} , and the magnetic island. The plasma current is 1.0 MA and the oxygen impurity content is 0.5 % . The gas-puffing starts at 1.0 sec and the volume-averaged-density $\overline{n}_e$ increases with a constant rate. The radiation loss increases almost proportionally to the square of the density. When the radiation loss becomes comparable to the joule heating power (t = 2.1 sec), the current channel starts to shrink and the q = 2 resonant surface moves outward. This shrink due to the surface radiation cooling destabilizes the tearing modes, and causes the overlapping of the 2/1 and 3/2 magnetic island at t = 3.2 sec. This critical density where the overlapping occurs (in this calculation, $< n_e > = 3.4 \times 10^{19}$ m^{-3}) are found for the various plasma current, the various content and impurity species. The calculated profiles of the electron temperature, $T_e (r)$, the electron density, $n_e (r)$, and the radiation power, $P_r (r)$ at the three different phases are shown in Fig. 7. The plasma with the moderate radiation power has the small width of the 2/1 island, as shown in Fig. 7 (a), because the q = 2 resonant surface is in the interior region of the plasma due to the high-q discharge. Fig. 7 (b) shows

that the plasma edge is sliced off by the radiation loss comparable to the joule input power. Fig. 7 (c) shows the plasma parameters just before the disruption. The time evolution of the current density is shown in Fig. 8. The current density in the central region is limited by the sawtooth oscillation. On the other hand, the current channel becomes narrow by the radiation cooling. As a result, the flattening region of m = 1 mode extends to outward. This change in the current density profile destabilizes the m/n = 2/1 and 3/2 tearing modes. Therefore, the sawtooth oscillation plays an important role in the occurrence of a major disruption.

The simulation results with $I_p = 2$ MA and oxygen content 2 % are shown in Figs. 9 and 10. Since the q = 2 resonant surface is close to the radiation region, a little shrink of the current channel leads to the overlapping. It occurs when the ratio of the radiation power to the joule input power, P_{rad} / P_{joul} reaches 0.9, as shown in Fig. 10. This ratio at the overlapping is somewhat lower, compared with that of the high-q discharge.

We also investigate the density limit of the plasma with the heavy metal impurity. Figures 11 and 12 shows the simulation results with the Molybdenum content of 0.01 % and the plasma current of 1 MA. It should be noted that the radiation profile is very different from the oxygen. (c.f. Fig. 7 and Fig. 10). The large radiation loss exists in the interior region of the plasma. Therefore, the current channel starts to shrink when the ratio of P_{rad} / P_{joul} reaches 0.85, while the ratio of P_{rad} / P_{joul} at the start of the shrink is nearly 1.0 for the light impurity case, as shown in Fig. 6.

We summarize the critical density calculated as a function of the plasma current for the oxygen impurity content from 0.5 % to 2 % and the titanium content of 0.05 % in Fig. 13. The I_p dependence of the maximum density qualitatively agrees with the experimental results. The content of 2 % oxygen, 0.5 % and 0.05 % correspond to the $Z_{eff} = 1.8$, 1.4 and 1.2, respectively. The value of the density limit calculated is smaller than that of the experimental observation for the plasma with the $Z_{eff} = 2 \sim 3$. As the impurity mass increases, the density limit has a weak current dependence since the radiation region extends to the inwards of the plasma due to the high ionization potential. The density limit

strongly depends on the shaping factor , C_v used in the calculation. Fig. 14 show that the density limit increases with C_v . The parameter of $I_p = 2$ MA and the oxygen impurity content of 2 % is used in these calculations. The plasma parameter and the impurity density profile calculated for C_v = 1.0 and 2.0 are shown in Figs. 15 (a) and (b) , respectively. As the shaping factor increases, the oxygen diffuses towards the inner region where the electron temperature is higher than the ionization potential and the radiation loss decreases. Thereby the overlapping occurs at high density for the large value of C_v. The discrepancy between the simulation and the experimental data may be explained by the anomalous enhancement of C_v in the peripheral region, not in the bulk region because the impurity transport analysis suggest that the shaping factor in the bulk plasma is nearly 0 in JT-60 Ohmic plasma [23].

4. Summary and Discussion

We have investigated the major disruption for the low-q operation and high density operation using the criterion of the overlapping of the 2/1 and 3/2 magnetic islands or the contact of the large 2/1 island with a limiter and obtained the following conclusions.

Low-q operation

(1) The control of the current rise is required for low-q operation.
(2) Fast current rise leads to the contact of m/n = 2/1 island with a limiter, or the overlapping 2/1 island with 3/2 island.
(3) The current rise rate must be lower than 0.75 MA/s for stable operation.
(4) It is possible to increase the current rise rate by the carefully controlled gas-puffing to suppress the skin current during the current rise.

High density operation

(1) The calculated result of density limit qualitatively agrees with experimental data

strongly depends on the shaping factor , C_v used in the calculation. Fig. 14 show that the density limit increases with C_v . The parameter of $I_p = 2$ MA and the oxygen impurity content of 2 % is used in these calculations. The plasma parameter and the impurity density profile calculated for C_v = 1.0 and 2.0 are shown in Figs. 15 (a) and (b) , respectively. As the shaping factor increases, the oxygen diffuses towards the inner region where the electron temperature is higher than the ionization potential and the radiation loss decreases. Thereby the overlapping occurs at high density for the large value of C_v. The discrepancy between the simulation and the experimental data may be explained by the anomalous enhancement of C_v in the peripheral region, not in the bulk region because the impurity transport analysis suggest that the shaping factor in the bulk plasma is nearly 0 in JT-60 Ohmic plasma [23].

4. Summary and Discussion

We have investigated the major disruption for the low-q operation and high density operation using the criterion of the overlapping of the 2/1 and 3/2 magnetic islands or the contact of the large 2/1 island with a limiter and obtained the following conclusions.

Low-q operation

(1) The control of the current rise is required for low-q operation.
(2) Fast current rise leads to the contact of m/n = 2/1 island with a limiter, or the overlapping 2/1 island with 3/2 island.
(3) The current rise rate must be lower than 0.75 MA/s for stable operation.
(4) It is possible to increase the current rise rate by the carefully controlled gas-puffing to suppress the skin current during the current rise.

High density operation

(1) The calculated result of density limit qualitatively agrees with experimental data

(2) Reduction of impurity content is important for high density operation.

(3) The sawtooth which limits the current density at the plasma center plays an important role in the major disruption.

(4) Impurity transport in the peripheral region which include the recycling model is important for the quantitative comparison with experimental data.

As the first step to comprehend a major disruption, we are concentrated on the joule heated plasma. We conclude that the criteria used in our calculation is justified for a occurrence of a major disruption. Now we are proceeding further with this work, i.e. the density limit for the additional heated plasma or the pellet injected plasma. The additional heating power can prevent the radiation collapse and the density limit is expected to increase by a factor of 2 ~ 3. The pellet injection can increases the density in the central region without the edge cooling, in contrast with the strong gas puffing, and attain the high density operation.

Acknowledgments

The authors would like to express the gratitudes to Drs. M. Yoshikawa, M. Tanaka and S. Tamura for their continuous encouragements.

(2) Reduction of impurity content is important for high density operation.

(3) The sawtooth which limits the current density at the plasma center plays an important role in the major disruption.

(4) Impurity transport in the peripheral region which include the recycling model is important for the quantitative comparison with experimental data.

As the first step to comprehend a major disruption, we are concentrated on the joule heated plasma. We conclude that the criteria used in our calculation is justified for a occurrence of a major disruption. Now we are proceeding further with this work, i.e. the density limit for the additional heated plasma or the pellet injected plasma. The additional heating power can prevent the radiation collapse and the density limit is expected to increase by a factor of 2 ~ 3. The pellet injection can increases the density in the central region without the edge cooling, in contrast with the strong gas puffing, and attain the high density operation.

Acknowledgments

The authors would like to express the gratitudes to Drs. M. Yoshikawa, M. Tanaka and S. Tamura for their continuous encouragements.

References

[1] MURAKAMI,M., CALLEN,J.D., BERRY,L.A., Nucl. Fusion 16 (1976) 347.

[2] PAUL,J.W.M., AXON,K.B., BURT,J., et al., in Plasma Physics and Controlled Nuclear Fusion Research (Proc. 6 th Int. Conf. Berchtesgaden, 1976) Vol. 2, IAEA, Vienna (1977) 269.

[3] SYKES,A and Wesson,J.A., Phys. Rev. Lett. 44 (1980) 1215.

[4] WADDEL,B.V., CARRERAS,B., HICKS,H.R., HOLMES,J.A., Phys. Fluids 22 (1979) 896.

[5] HICKS,H.R., CARRERAS,B.A., HOLMES,J.A. and LYNCH,V.E., Nucl. Fusion 22 (1982) 117.

[6] SHIMIZU,K., SHIRAI,H., HIRAYAMA,T., AZUMI,M., TAKIZYKA,T., TANI.K., Proc. 12 th European Conf. on Controlled Fusion and Plasma, Budapest, 1985, Vol. 1, p179.

[7] HIRAYAMA,T., SHIRAI,H., SHIMIZU,K., AZUMI,M., TAKIZUKA,T., J. Nucl. Mater 145-147 (1987) 854.

[8] JT-60 Team, Japan Atomic Energy Research Institute, Japan, Report No. JAERI-M 87-009 (1887).

[9] CHANG,C.S. and HINTON,F.L., Phys. Fluids 25 (1982) 1493.

[10] BLACKWELL,B., FIORA,C.L., GANGY,R., GONDHALEKAR,A., et al., in Plasma Physics and Controlled Nuclear Fusion Research (Proc. 9 th Int. Conf. Baltimore, 1982) Vol. 2, IAEA, Vienna (1983) 27.

[11] HIRAYAMA,T. et al.., GA-A17406 (1984).

[12] HOULSE,R.A., Technol./Fusion 3 (1983) 259.

[13] KANEKO,Y., et al., Nagoya University, Nagoya, Japan, Report No. IPPJ-AM-15 (1980).

[14] FONCK,R.J. and HOULSE,R.A., Phys. Rev. Lett. 52 (1984) 530.

[15] FURTH,H.P., RUTHERFORD,P.H., SELBERG,H., Phys. Fluids (1963) 459.

[16] RUTHERFORD,P.H., Phys. Fluids 16 (1973) 1903.

[17] CARRERAS,B., WADDEL,B.V., and Hicks,H.R., Nucl. Fusion 19 (1979) 1423.

[18] WADDEL,B.V., JHONS,G.L., CALLEN,J.D., HICKS,H.R., ORNL/TM-5840 (1977).

[19] KADOMTES,B.B., Fizika Plazmy (1975) 710.

[20] SHIRAI.H, NAGASHIMA,K., NISHITANI,T. and JT-60 team, JAERI-M 87-014 (1987).

[21] TURNER,M.F. and WESSON,J.A., Nucl. Fusion 22 (1982) 1069.

[22] OZEKI,T., private communication (1989).
NINOMIYA,H., YOSHINO,R., AKIBA,M., ANDO,T., et al., Paper No. A-II-3, in Plasma Physics and Controlled Nuclear Fusion Research (Proc. 12 th Int. Conf. Niece, 1988) .

[23] JT-60 team, in Plasma Physics and Controlled Nuclear Fusion Research (Proc. 11 th Int. Conf. Tokyo, 1986) Vol. 1, IAEA, Vienna (1987) 217.

Table 1 Calculation parameters

Major radius	$R = 3.03$ m
Minor radius	$a = 0.95$ m
Toroidal field	$B_t = 4.5$ T
Plasma current	$I_p = 1 - 2.7$ MA
Electron thermal diffusivity	$\chi_e = 4.4 \times 10^{20}\, r / R^2\, n_e$
Ion thermal diffusivity	$\chi_i = 3 \times \chi_i^{CH}$
Particle diffusion coefficient	$D_e = 1.0 \times 10^{19} / n_e$

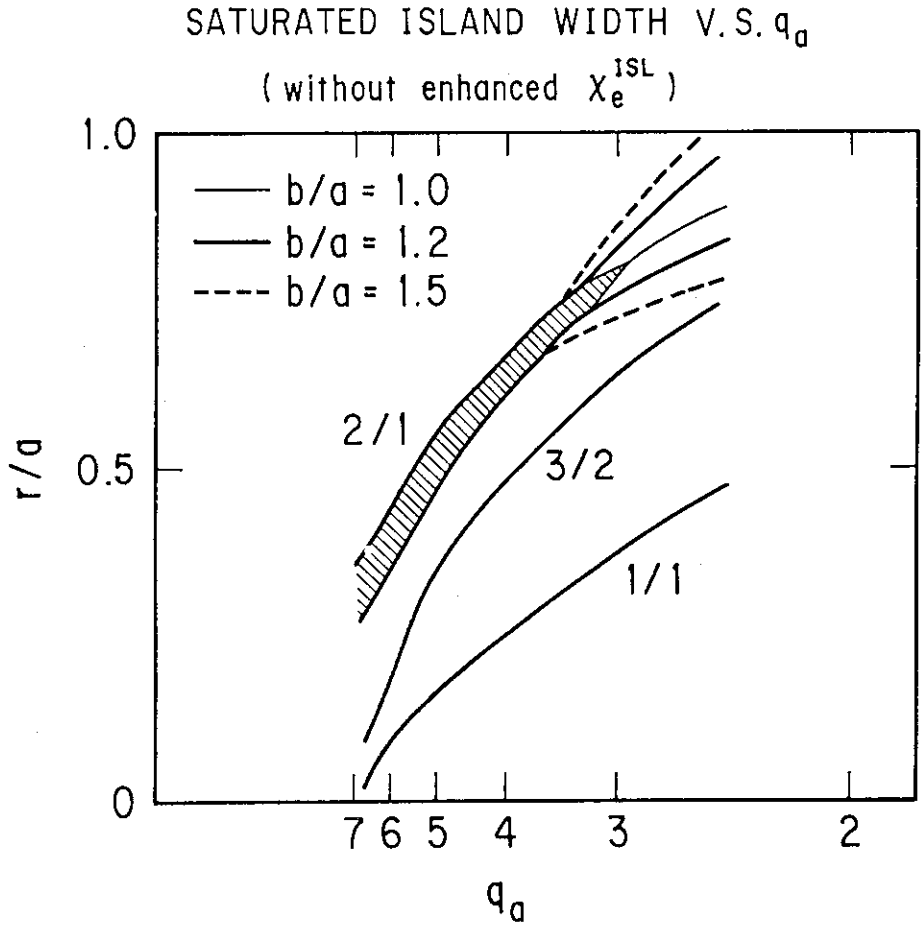

Fig. 1 Saturated island width as a function of the safety factor.

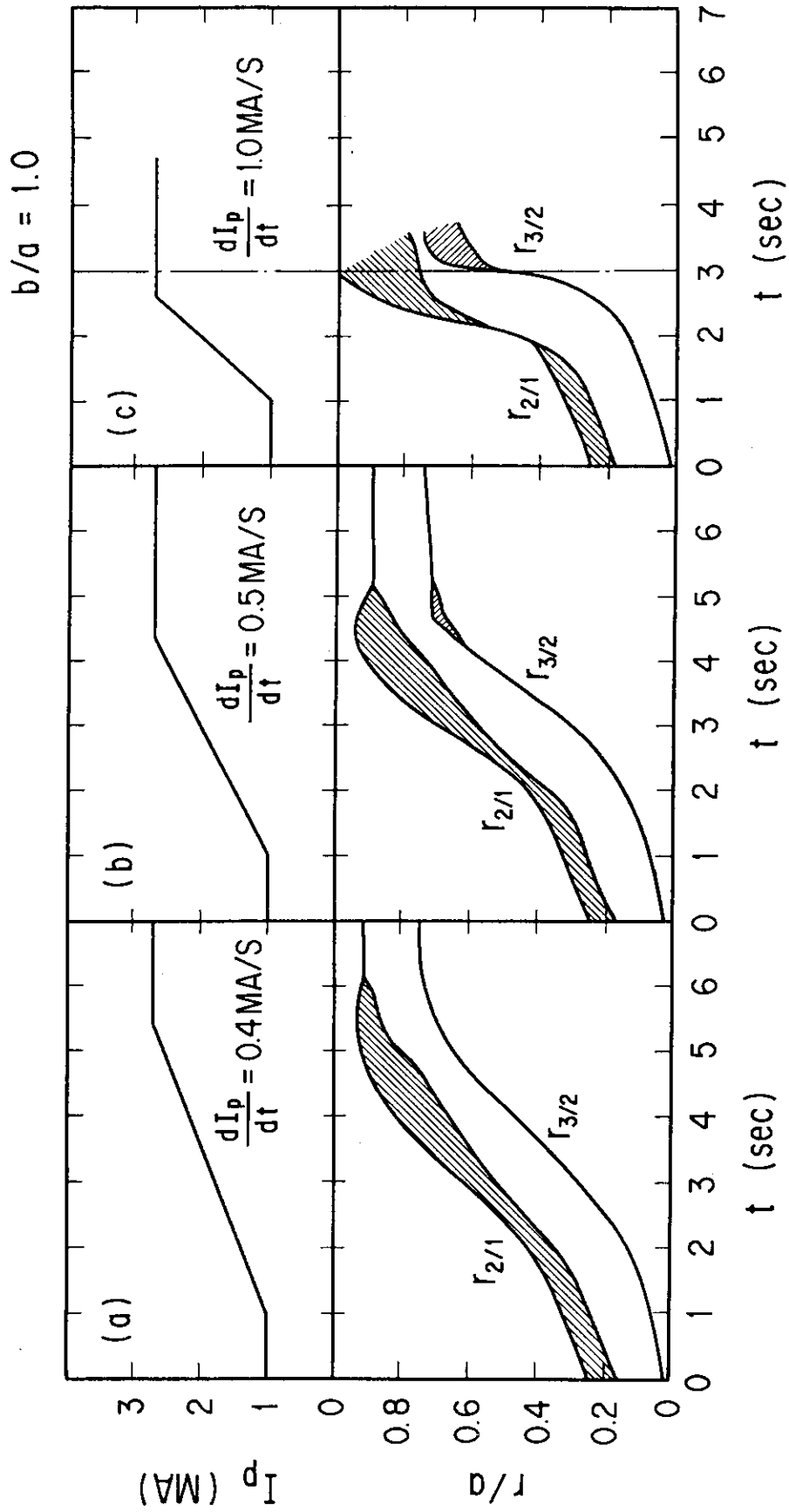

Fig. 2 Time evolutions of magnetic islands during current rise up phase for three different current rises. In these calculations the electron thermal conductivity inside the island is not enhanced and the conducting wall is placed at the plasma surface.

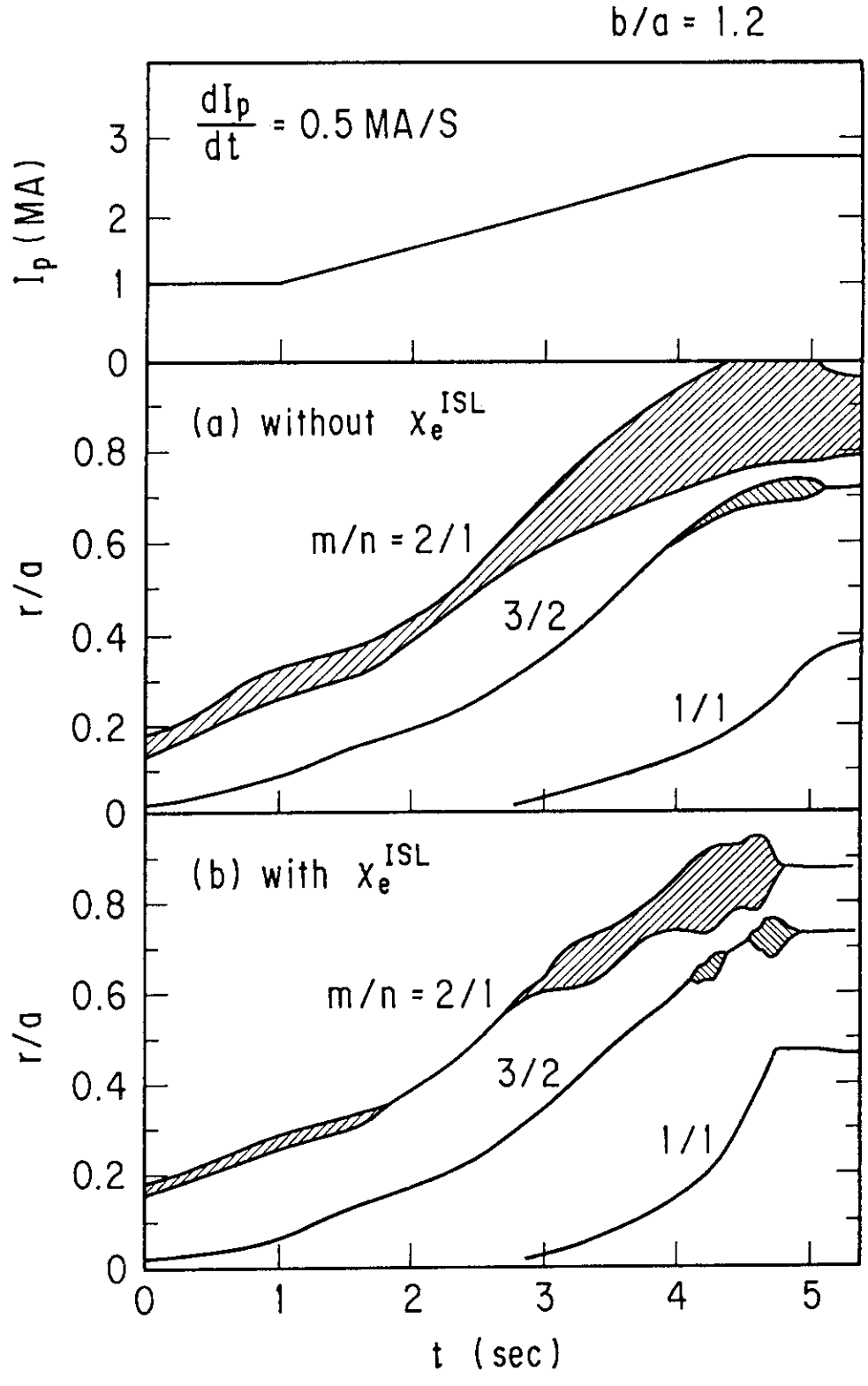

Fig. 3 The effect of enhanced thermal conductivity inside the island. The current rise rate is $dI_p / dt = 0.5$ MA/s . The wall position is taken to be b / a = 1.2 hereafter.

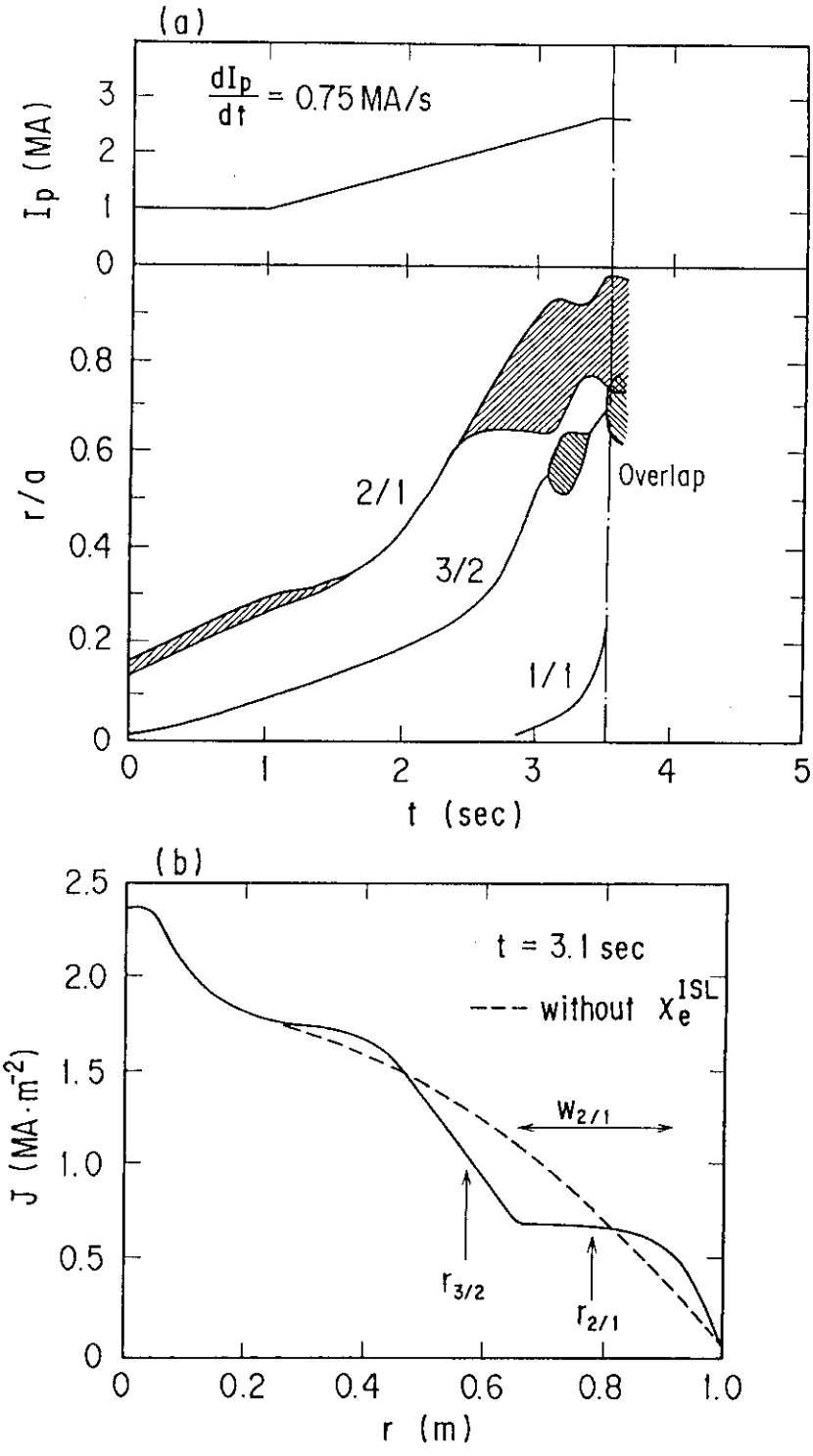

Fig. 4 Time evolution of magnetic islands calculated with the effect of χ_e^{ISL} for $dI_p / dt = 0.75$ MA/s . The broken line is the current density profile without the effect of χ_e^{ISL} . The large island of the 2/1 mode produce the sharp gradient at the q = 3/2 resonant surface, the 3/2 mode grows up explosively and then a major disruption occurs at t = 3.5 sec.

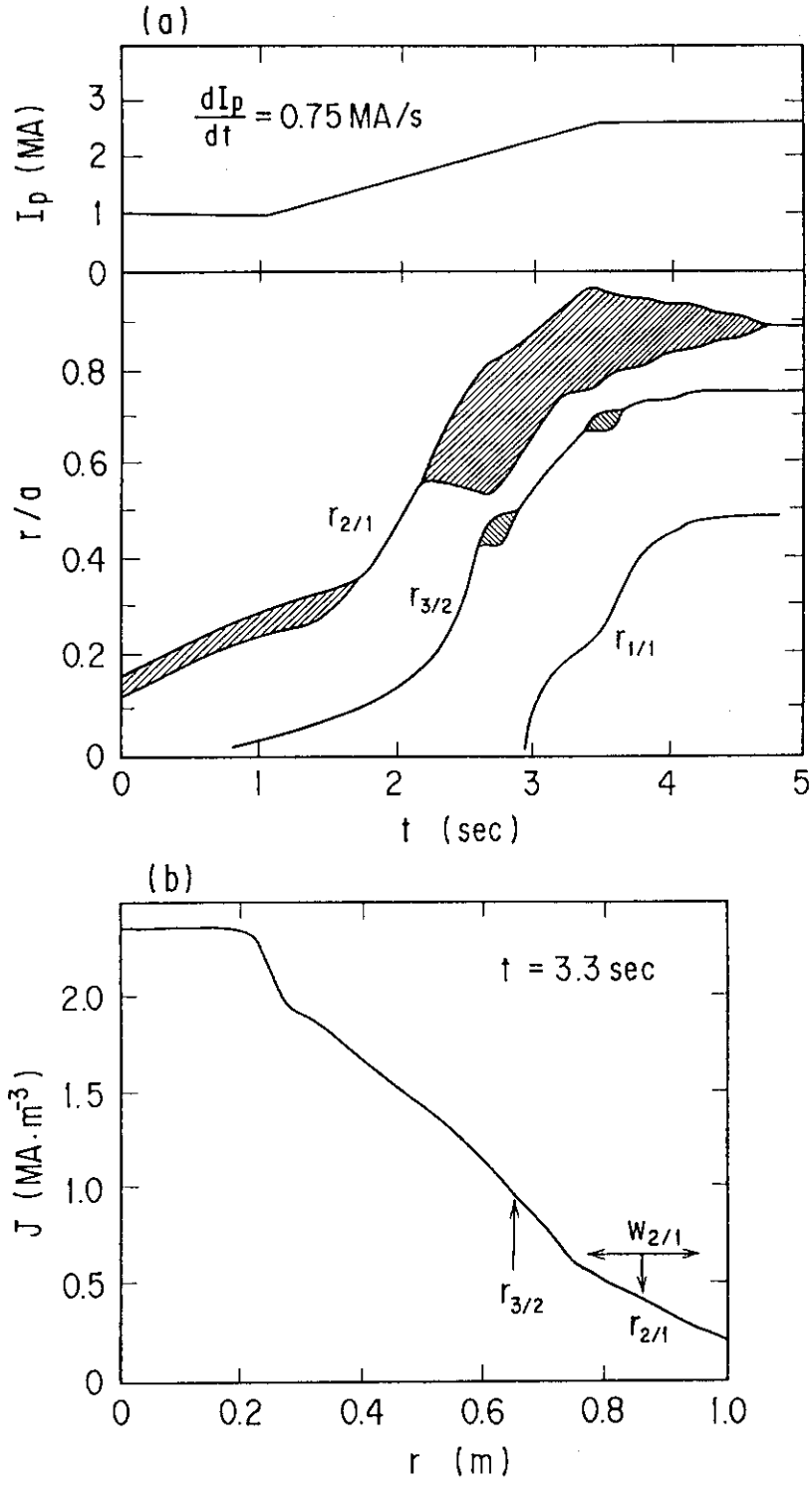

Fig. 5 The effect of the edge electron temperature. In this calculation, the transport equation including the scrape-off region is solved. The high edge temperature, which is self-consistently determined by the balance of the parallel loss and the diffusion, suppress the skin current and the disruption can be avoided.

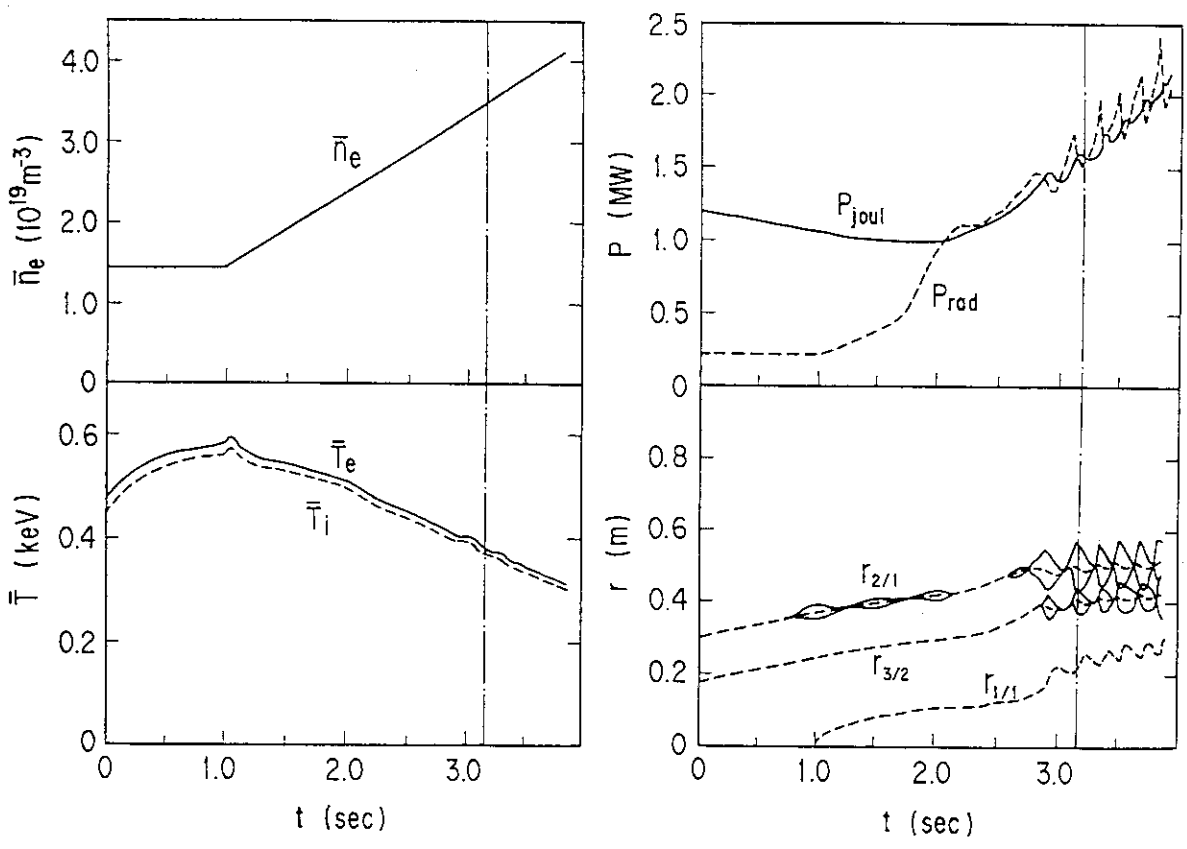

Fig. 6 The time evolution of the plasma parameter (the volume-averaged density $\bar{n}_e$, the particle-averaged electron and ion temperature $\bar{T}_e$, $\bar{T}_i$,the joule input power P_{joul}, the impurity radiation loss P_{rad} and the magnetic island) calculated for $I_p = 1$ MA with the oxygen impurity content of 0.5 %. The overlapping of the magnetic islands occurs when the volume-averaged density reaches $\bar{n}_e = 3.4 \times 10^{19}$ m^{-3} .

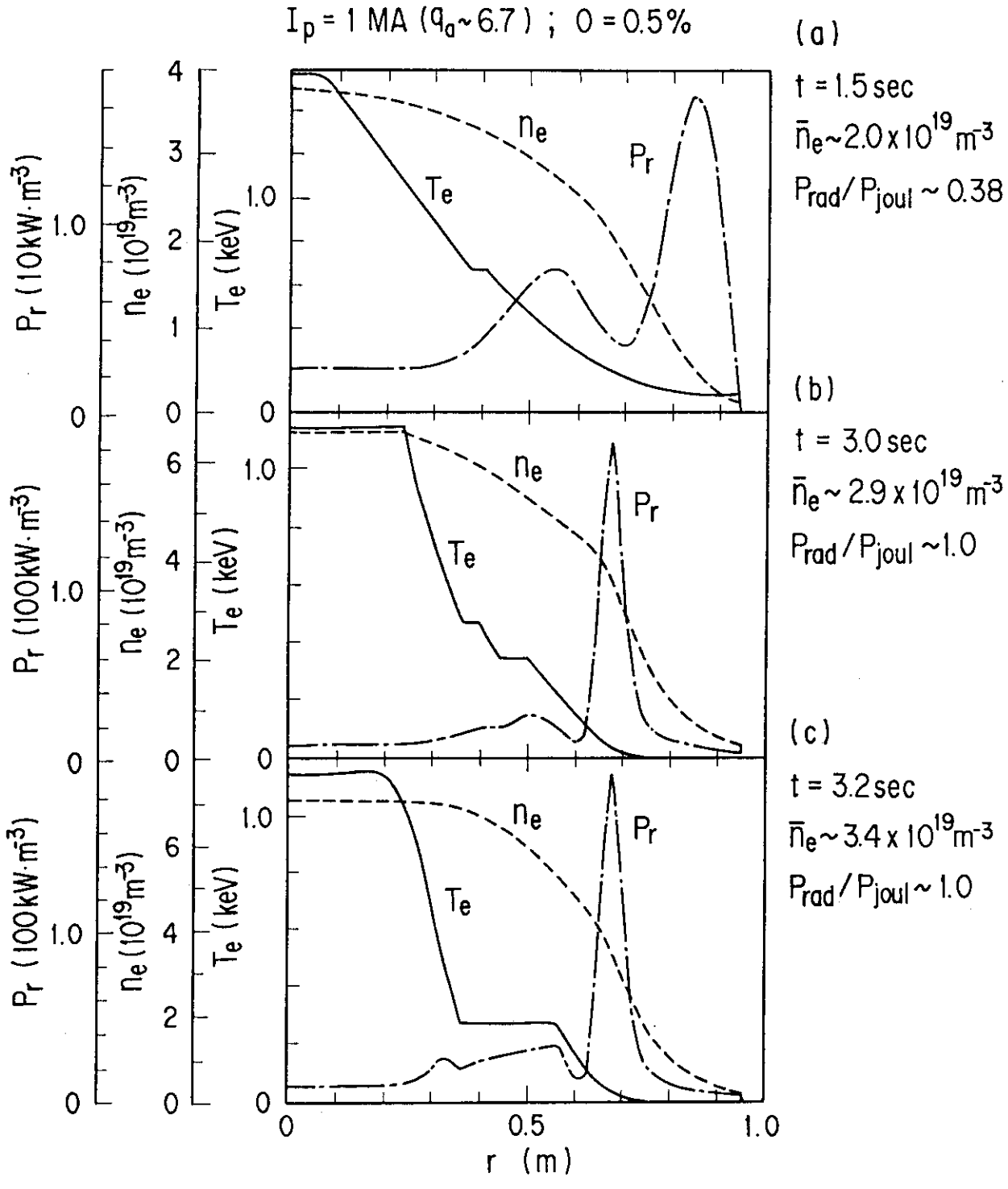

Fig. 7 The profiles of the electron temperature $T_e(r)$, the electron density $n_e(r)$ and the radiation power $P_r(r)$ calculated for $I_p = 1$ MA with the oxygen impurity content of 0.5 %.

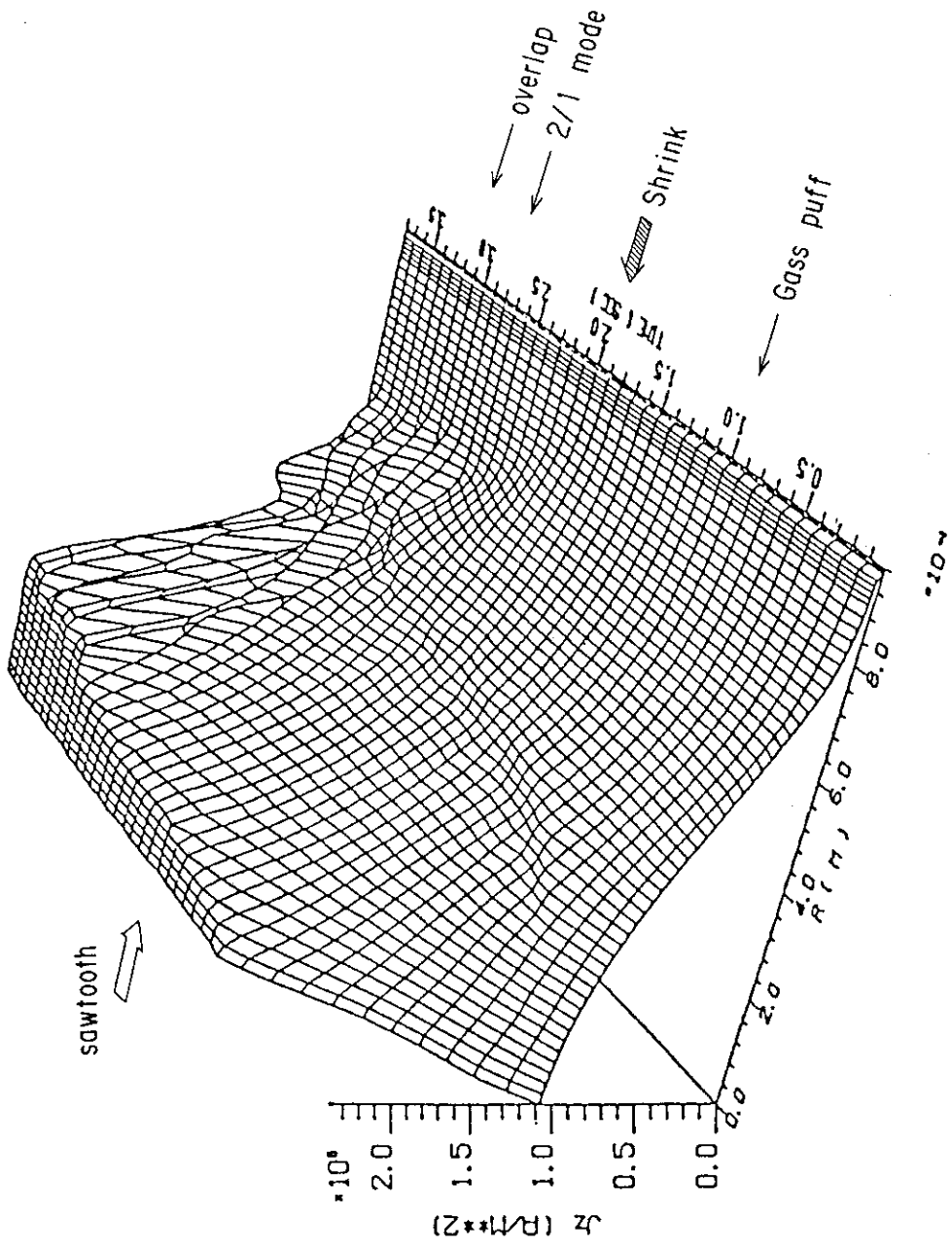

Fig. 8 The time evolution of the current density profile calculated for I_p = 1 MA with the oxygen impurity content of 0.5 %. The sawtooth oscillation which limits the current density at the plasma center plays an important role in driving the tearing mode unstable, especially the 3/2 mode which is destabilized under the limited condition.

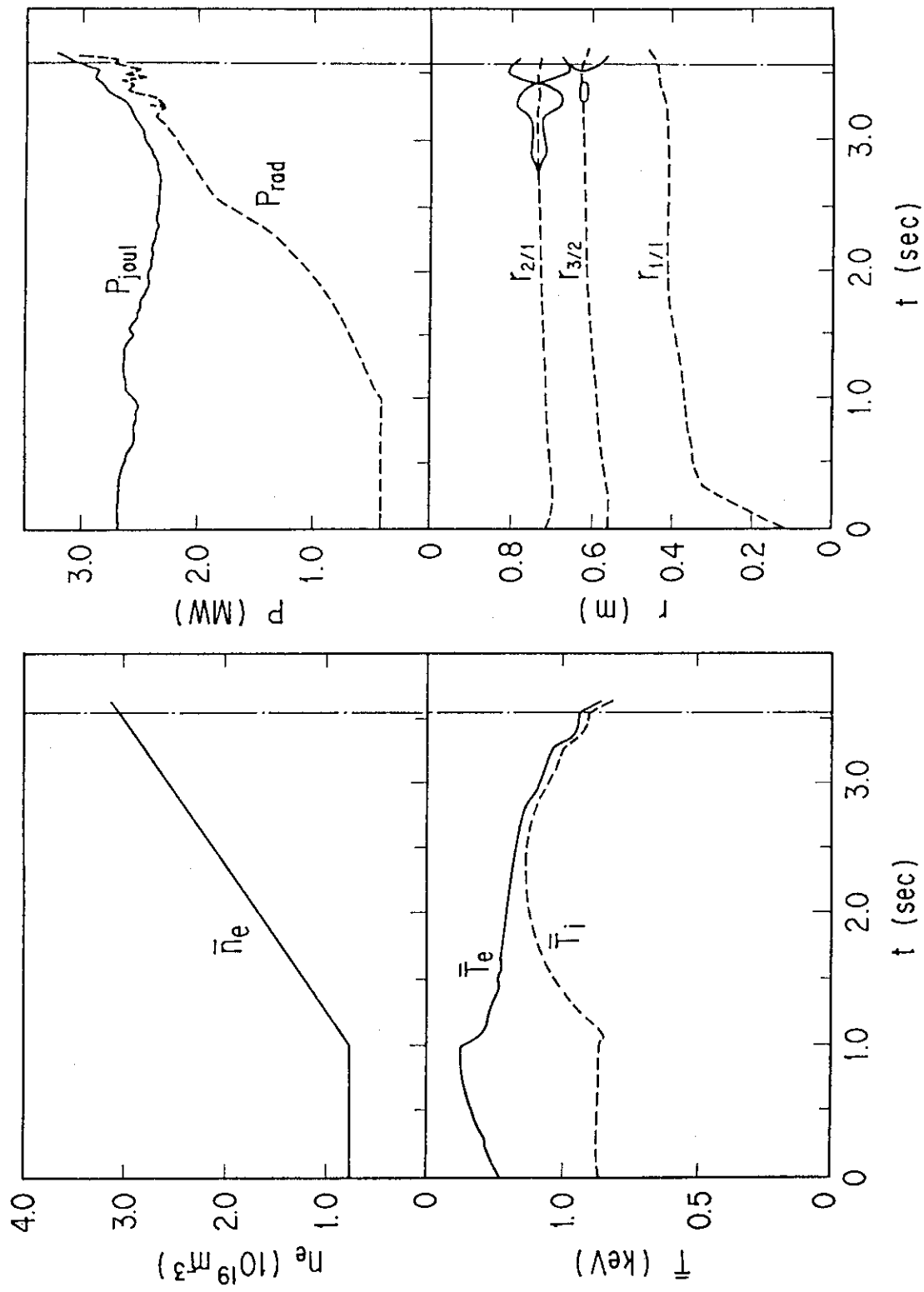

Fig. 9 The time evolution of the plasma parameter calculated for $I_p = 2$ MA with the oxygen impurity content of 2 %.

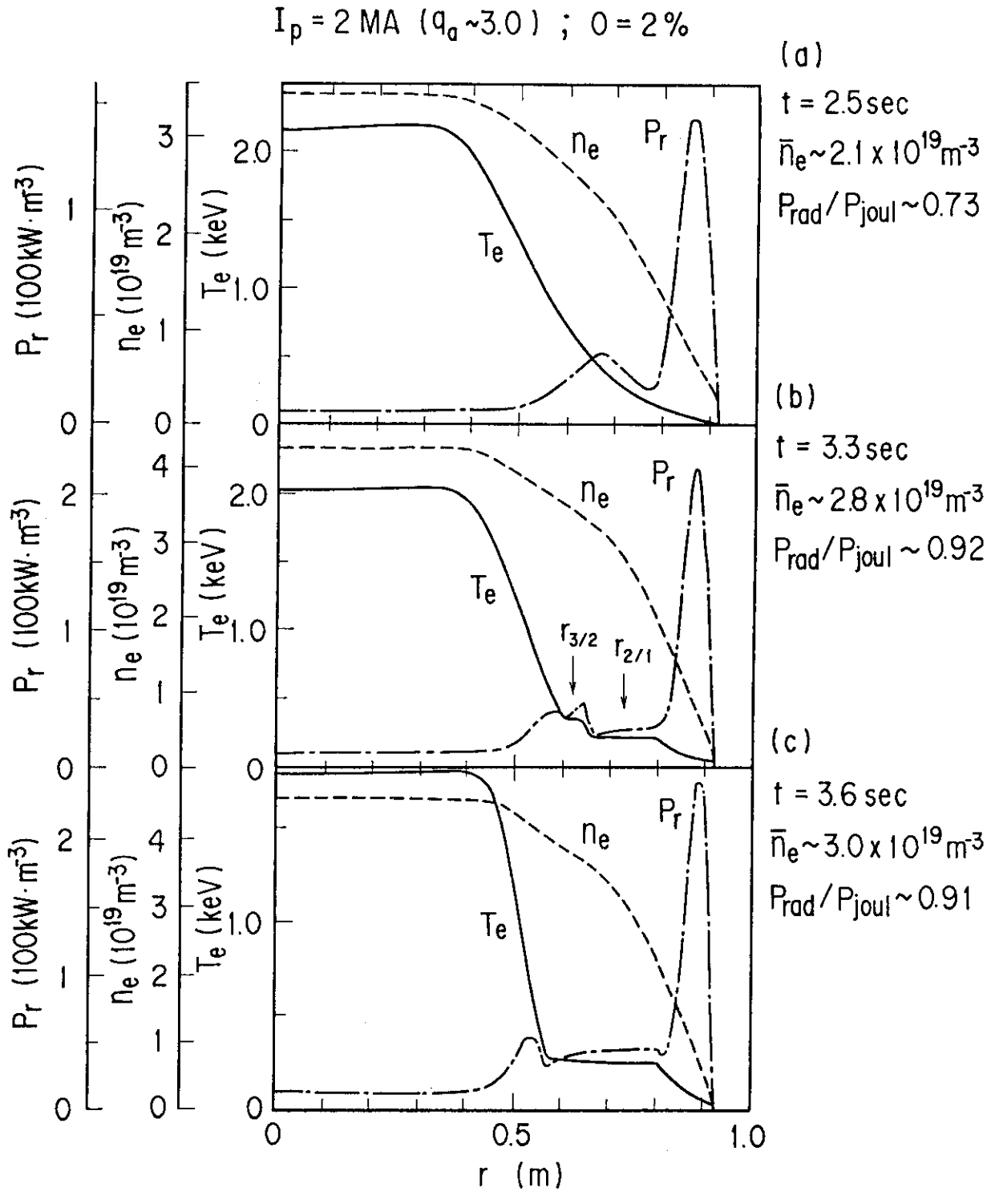

Fig. 10 The profiles of the plasma parameter calculated for I_p = 2 MA with the oxygen impurity content of 2 % in three different phases.

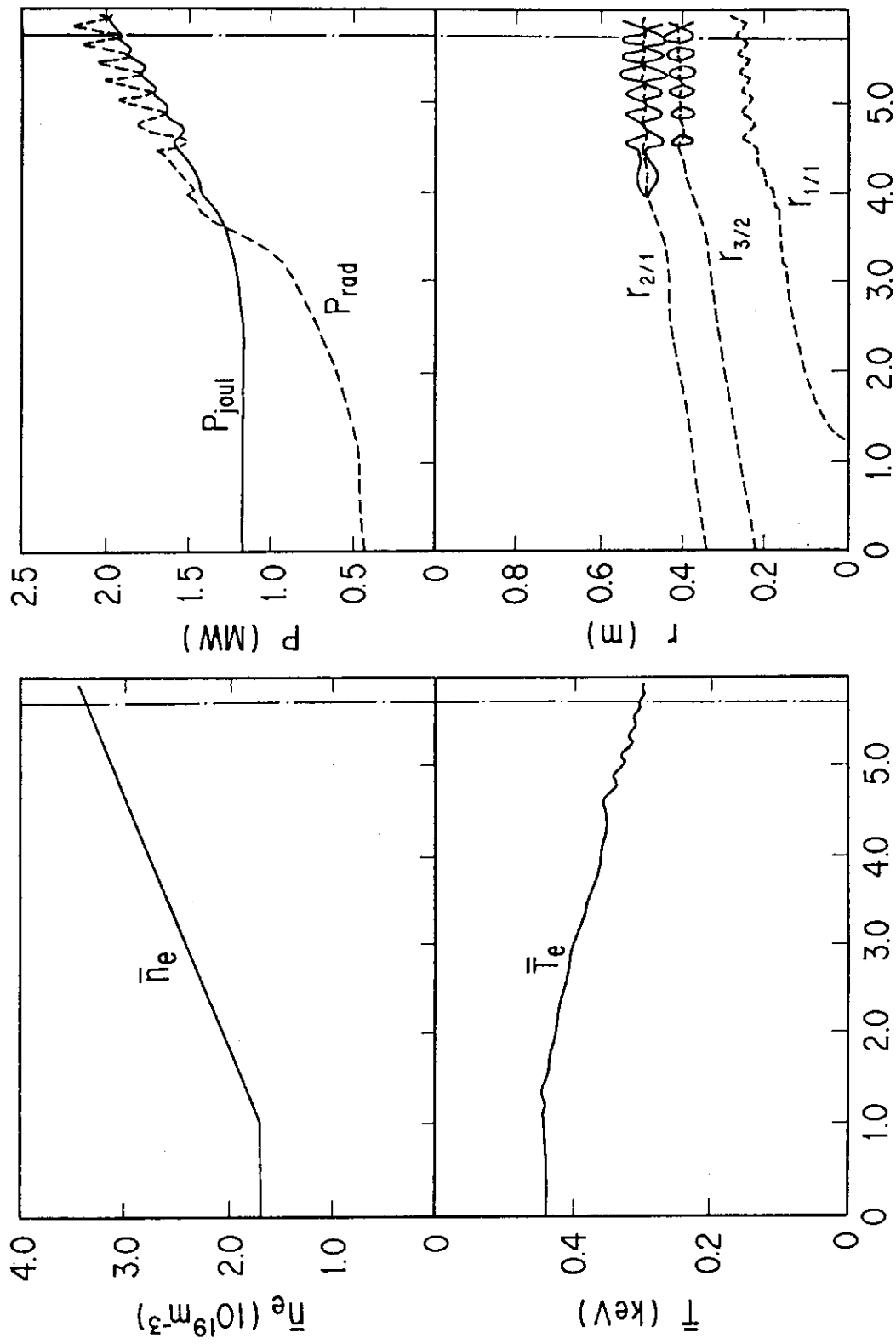

Fig. 11 The time evolution of the plasma parameter calculated with I_p = 1 MA with the molybdenum impurity content of 0.01 %.

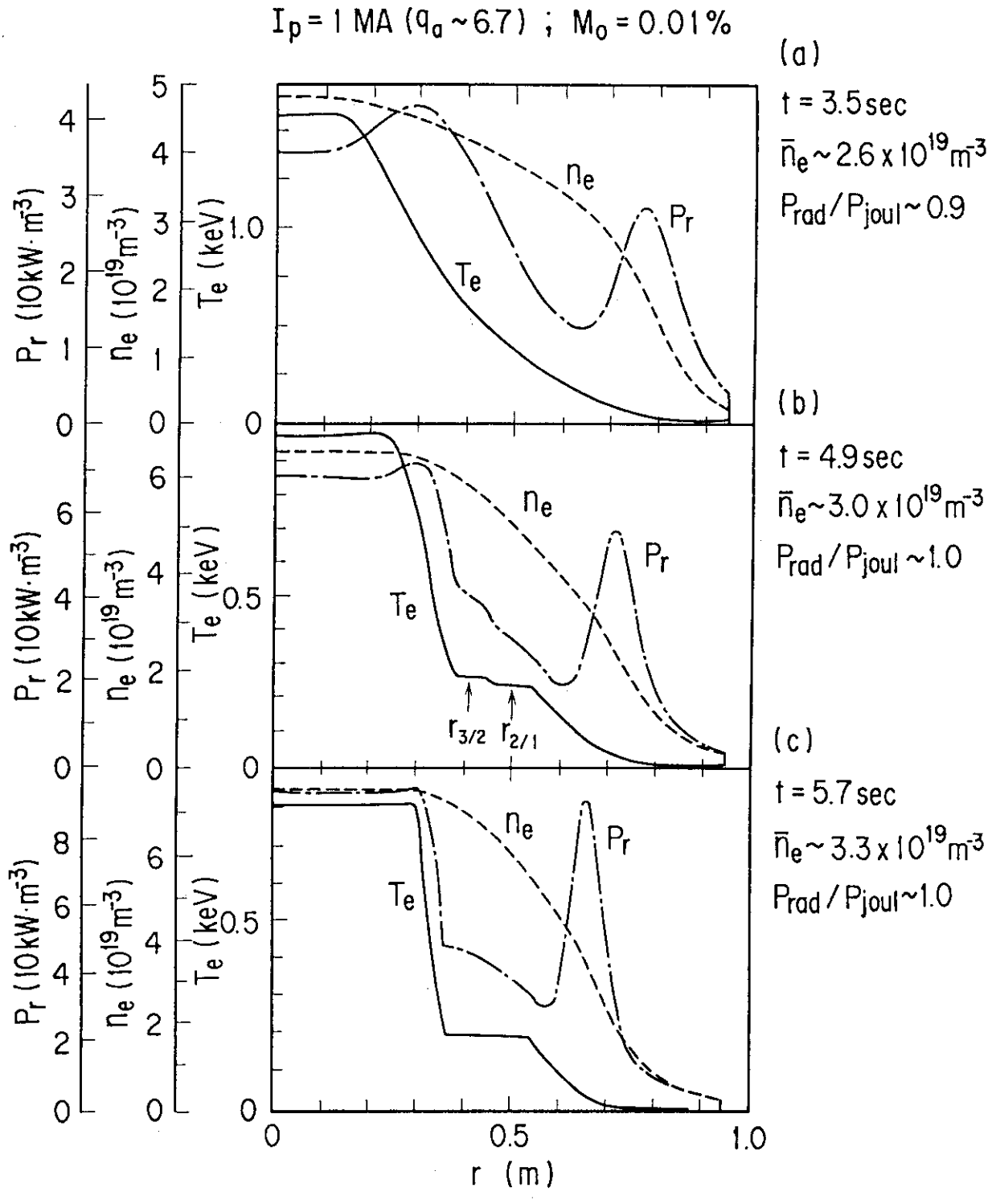

Fig. 12 The profiles of the plasma parameter calculated for I_p = 1 MA with the molybdenum impurity content of 0.01 %.

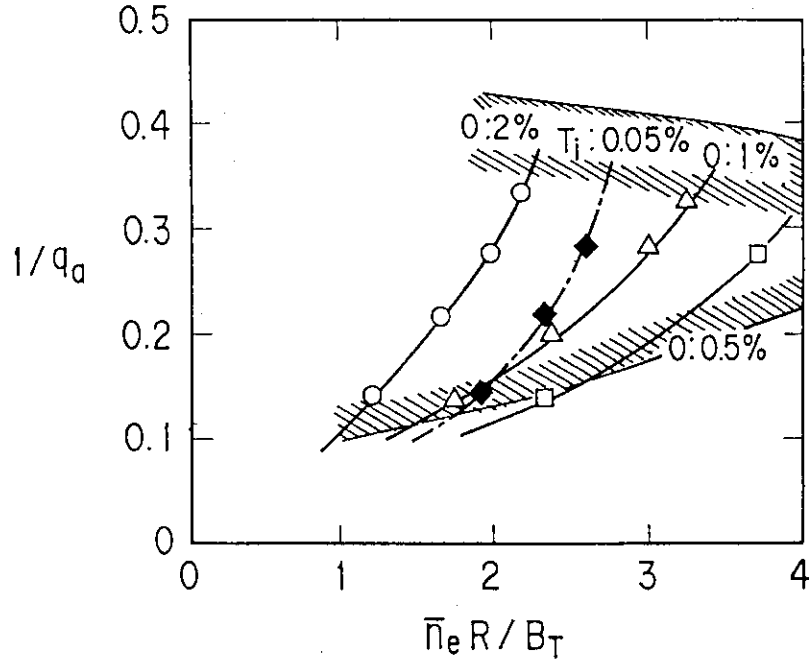

Fig. 13 The critical density when the overlapping occurs as a function of the plasma current for the oxygen impurity content from 0.5 % to 2 % and the titanium impurity of 0.05 %. The shaded region shows the operation region obtained experimentally. The I_p dependence of the density limit agrees with the experimental data.

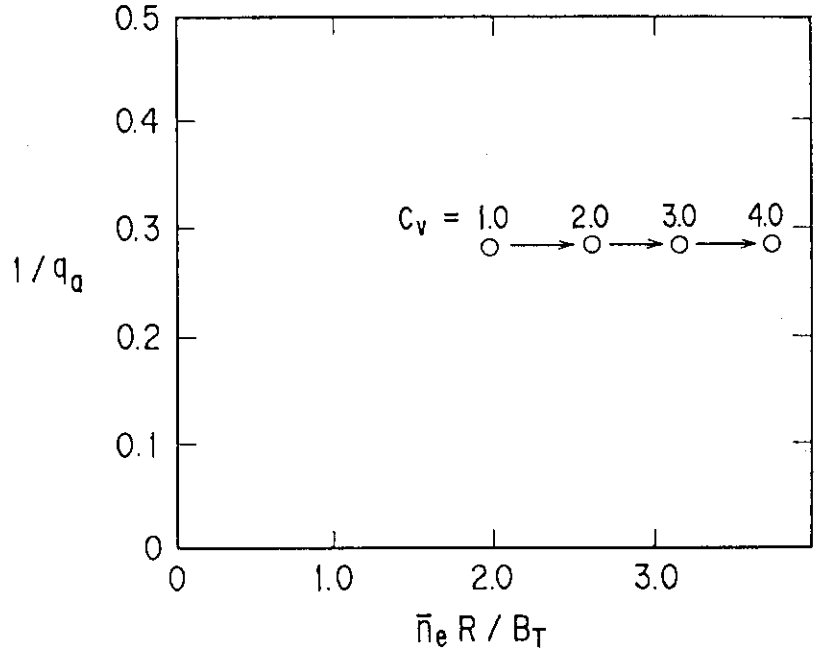

Fig. 14 The density limit calculated for the various values of the shaping factor C_v . The calculation parameters of $I_p = 2$ MA and the oxygen impurity content of 2 % is used.

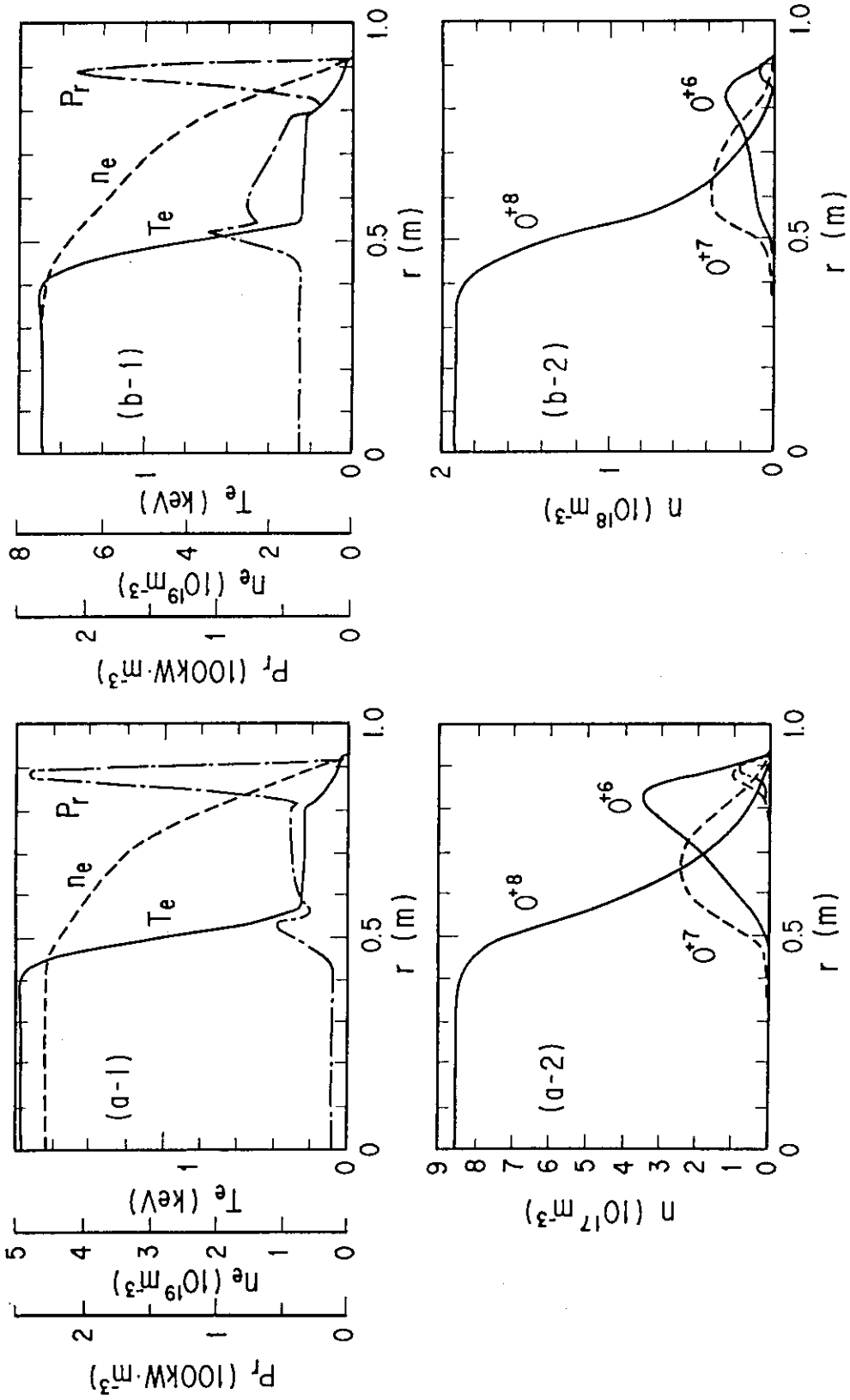

Fig. 15 The profiles of the plasma parameter when the disruption occurs. In the simulation of (a) and (b), the shaping factor C_v is taken to be 1.0 and 2.0, respectively.